Sound attenuation enhancement of acoustic meta-atoms via coupling

Felix Kronowetter ; Lisa Pretsch; Yan Kei Chiang; Anton Melnikov; Shahrokh Sepehrirahnama; Sebastian Oberst; David A. Powell; Steffen Marburg

Check for updates

CrossMark

View Online

Export Citation

CrossMark
click for updates
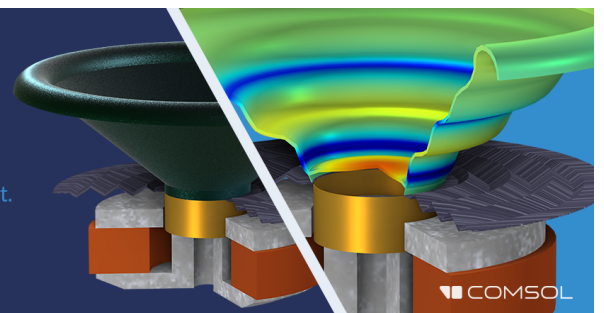
Sound attenuation enhancement of acoustic meta-atoms via coupling[a)]

Felix Kronowetter,[1,b)] (iD) Lisa Pretsch,[2] Yan Kei Chiang,[3] Anton Melnikov,[4] Shahrokh Sepehrirahnama,[5] Sebastian Oberst,[5] David A. Powell,[3] and Steffen Marburg[1] (iD)

[1]*Chair of Vibro-Acoustics of Vehicles and Machines, Department of Engineering Physics and Computation, Technical University of Munich, TUM School of Engineering and Design, Munich, Germany*

[2]*Associate Professorship of Computational Solid Mechanics, Department of Engineering Physics and Computation, Technical University of Munich, TUM School of Engineering and Design, Munich, Germany*

[3]*School of Engineering and Information Technology, University of New South Wales, Northcott Drive, Canberra, Australian Capital Territory 2600, Australia*

[4]*Bosch Sensortec, Dresden, Germany*

[5]*School of Mechanical and Mechatronic Engineering, Centre for Audio, Acoustics and Vibration, Faculty of Engineering and IT, University of Technology Sydney, Sydney, Australia*

ABSTRACT:

Arrangements of acoustic meta-atoms, better known as acoustic metamaterials, are commonly applied in acoustic cloaking, for the attenuation of acoustic fields or for acoustic focusing. A precise design of single meta-atoms is required for these purposes. Understanding the details of their interaction allows improvement of the collective performance of the meta-atoms as a system, for example, in sound attenuation. Destructive interference of their scattered fields, for example, can be mitigated by adjusting the coupling or tuning of individual meta-atoms. Comprehensive numerical studies of various configurations of a resonator pair show that the coupling can lead to degenerate modes at periodic distances between the resonators. We show how the resonators' separation and relative orientation influence the coupling and thereby tunes the sound attenuation. The simulation results are supported by experiments using a two-dimensional parallel-plate waveguide. It is shown that coupling parameters like distance, orientation, detuning, and radiation loss provide additional degrees of freedom for efficient acoustic meta-atom tuning to achieve unprecedented interactions with excellent sound attenuation properties.

© 2023 Author(s). All article content, except where otherwise noted, is licensed under a Creative Commons Attribution (CC BY) license (http://creativecommons.org/licenses/by/4.0/). https://doi.org/10.1121/10.0020570

(Received 17 March 2023; revised 5 June 2023; accepted 20 July 2023; published online 11 August 2023)

[Editor: Nicole Kessissoglou]   Pages: 842–851

I. INTRODUCTION

Acoustic metamaterials are artificial structures consisting of an arrangement of meta-atoms that can be used to control or manipulate the propagation of sound and elastic waves due to their exotic behavior (Cummer *et al.*, 2016; Deymier, 2013; Ma and Sheng, 2016; Zangeneh-Nejad and Fleury, 2019). The operating principle of meta-atoms is mostly based on local resonances leading to, for example, a negative effective mass density (Milton and Willis, 2007; Yao *et al.*, 2008), negative bulk modulus (Fang *et al.*, 2006), or negative refractive index (Pendry, 2000). Since meta-atoms are typically arranged close to each other, i.e., less than their operating wavelength, interaction such as longitudinal near-field coupling (Wang and Laude, 2017) and transverse coupling (Fu *et al.*, 2011) occur. In the context of the acoustics of a lossless medium, there is only pressure coupling. Such coupling and associated parameters can provide

additional degrees of freedom to tune the system, e.g., to enhance sound transmission (Yang *et al.*, 2015).

Coupling effects have been applied for the tuning of electro-magnetic metamaterials (Pendry *et al.*, 2006; Schurig *et al.*, 2006; Valentine *et al.*, 2009). Keiser *et al.* (2013) employed near-field interaction phenomena in the design of electro-magnetic metamaterials. Coupling between electro-magnetic metamaterial elements can have a significant impact on the behavior of the material as a whole (Liu *et al.*, 2009a). Especially for very closely arranged elements, it is no longer adequate to solely consider the averaged effect of the uncoupled resonators. Instead of treating the metamaterial as a continuous effective medium, the near-field interaction phenomena have to be considered. These phenomena give rise to various applications, like frequency tunable and broad bandwidth metamaterials (Keiser *et al.*, 2013; Liu *et al.*, 2009a). Powell *et al.* (2010) investigated the near-field interaction between split-ring resonators (SRRs) as resonant structures of a metamaterial. They found that modifications of the structures' relative orientation and separation affected the near-field interaction. Thereby, the metamaterial response can be tuned. In a subsequent paper, Powell *et al.* (2011)

---

examined the linear near-field interaction of a pair of SRRs on the same axis with varying relative angle and observed a crossing point between the symmetric and antisymmetric mode in the dispersion curve. The analysis of the (anti-) crossing behavior is based on the mode coupling model presented by Yakovlev and Hanson (2000). Studying a similar system, Liu et al. (2009b) found that with increasing twist angle the resonant modes converge, pass through an avoided crossing, and then diverge again. The acoustic counterpart to SRRs is Helmholtz resonators (Movchan and Guenneau, 2004).

Analogous coupling effects can be found in acoustics, more precisely, in the analysis of organ pipes. Existing studies on the interaction of organ pipes contribute useful findings that can be adapted to locally resonant structures. Two organ pipes sound in unison when close together, even if their natural frequencies differ slightly (Strutt, 2011). Fischer et al. (2016) investigated the mutual interaction of a pair of organ pipes experimentally and analytically. Sawicki et al. (2018) examined the effect of separation and frequency detuning of two coupled organ pipes on their synchronization behavior. Pikovsky et al. (2001) give a summary of the nonlinear principle of synchronization with applications in diverse fields of science, like engineering, biology, and social behavior. Although synchronization is based on non-linear effects, analogies can be extracted to explain the degeneracy of modes. With the aim to understand the interaction between close organ pipes, Johansson and Kleiner (2001) investigated the coupling effects of two Helmholtz resonators. They argue that the coupling mechanisms of organ pipes and Helmholtz resonators resemble each other. Despite different working principles, simple Helmholtz resonators thus present a good approximation for more complex organ pipes. Two Helmholtz resonators can be coupled via the surrounding air by bringing them close together.

Various studies on coupling of acoustic resonators in waveguides (Al Jahdali and Wu, 2018; Herrero-Durá et al., 2020; Wang and Laude, 2017; Zhou et al., 2018) have been reported. Recent publications (Cavalieri et al., 2019; Krasikova et al., 2022; Lee and Iizuka, 2019) apply coupling to acoustic metamaterials, whereby the interaction of local resonances within a unit cell—in a subwavelength region—is considered. Cavalieri et al. (2019) demonstrate that the combination of local resonators of different types combined with the periodicity of the system can lead to multiple coupled resonances to achieve broadband acoustic attenuation. The interaction of local resonances and Bragg scattering are investigated by Lee and Iizuka (2019). Krasikova et al. (2023) investigate the strong coupling between pairs of resonators within a unit cell and their influence on the dispersion curves and the transmission spectrum. Additionally, coupling is used for tuning acoustic lenses (Yang et al., 2015) and metagratings (Dong et al., 2017).

In this article, we investigate coupling of two C-shaped meta-atoms in a two-dimensional unbounded domain. Since almost all acoustic metamaterials can be thought of as arrayed coupled resonators, we refer to them as meta-atoms, even if

we consider only two of them (Belacel et al., 2017; Wu et al., 2017). Coupling between meta-atoms affects the total performance of periodic structures shown by Krasikova et al. (2023). The modal behavior of the system for varying parameters, like distance, orientation, detuning, and radiation losses, is studied. Fundamental effects are explained for a better understanding of the coupling mechanisms. We demonstrate how the sound attenuation of meta-atoms can be improved and adjusted using orientation and positioning as tunable parameters. In addition, we detune the resonance frequency of one of the resonators and present how the detuning affects the modal behavior. Furthermore, we show how increased radiation losses can counteract detuning concerning the interaction of the eigenfrequencies of the system. The numerical results are validated by experiments. A two-dimensional parallel-plate waveguide (Melnikov et al., 2019) is used for the evaluation of sound pressure fields of the acoustic meta-atoms. We demonstrate how coupling affects the performance of local resonances in terms of sound attenuation and hence, can provide an improved design of acoustic metamaterials.

II. NUMERICAL MODEL

Figure 1(a) shows the configuration of a pair of two-dimensional C-shaped Helmholtz resonators (Chalmers et al., 2009; Elford et al., 2011), within a rectangular acoustic domain surrounded by a perfectly matched layer. The rectangular domain with absorbing boundaries is chosen such that it resembles the waveguide used for experiments hereinafter presented. We denote the C-shapes' inner radius $r = 6\,\text{mm}$, the aperture width $w = 4\,\text{mm}$, and the thickness $t = 16\,\text{mm}$. The choice of the geometric dimensions of the C-shape depends on the following factors: the walls of the C-shape must be thick enough to be considered sound hard. We choose a wall thickness of 16 mm based on our experience from previous measurements. Furthermore, the eigenfrequencies of our system are determined by the dimensions and thus, the measurable frequency range (1000–2400 Hz) of the waveguide used in our experimental setup. The chosen aperture width of 6 mm is large compared to the expected boundary layer thickness of $\delta_\eta = \sqrt{2\eta/\rho_m \omega} \approx 0.05\,\text{mm}$ following the formulations in the book by Dukhin and Goetz (2002); nevertheless, we consider thermo-viscous losses in our simulations. Thermo-viscous boundary layer losses are significant for structures with narrow geometry features (Jiang et al., 2017; Jordaan et al., 2018). The inter-resonator distance is denoted l and is measured from the exterior of each resonator. Initially, both apertures face Γ_i with $\alpha = 90°$. All studies in this section are conducted as finite element simulations in COMSOL Multiphysics (COMSOL Inc., 2021), first in the form of modal analyses, then by the transmission response for harmonic excitation through a plane wave. The modal analysis of a single C-shape results in the complex individual eigenfrequency $f_c = 1960 + 82i\,\text{Hz}$. The real part of the complex eigenfrequencies $f_c = f + i\gamma$ is the resonant frequency f; the imaginary part γ characterizes the radiation loss (Baydoun and Marburg, 2020;

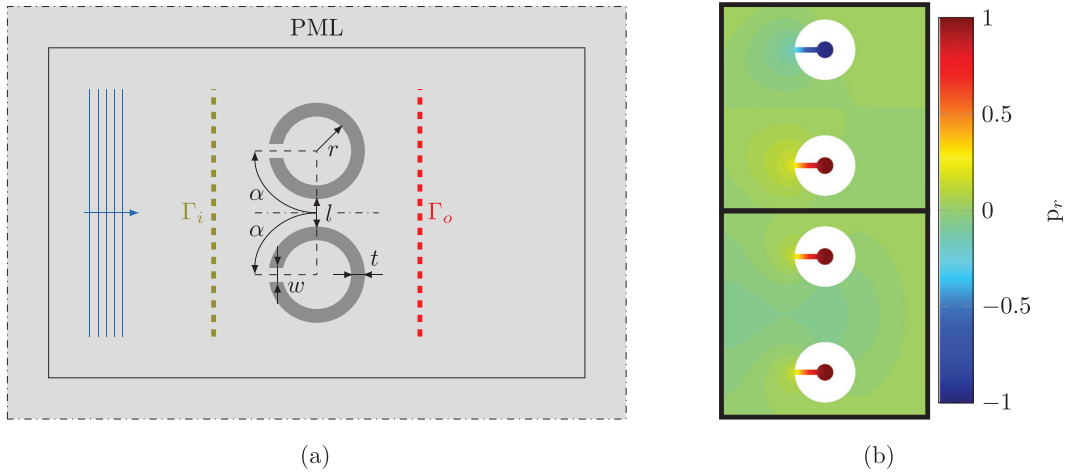J. Acoust. Soc. Am. **154** (2), August 2023

Kronowetter et al. 843

FIG. 1. (Color online) (a) Numerical setup. The schematic of the resonator pair geometry and dimensions, specified by inner radius r, aperture width w, wall thickness t, and inter-resonator distance l in a two-dimensional unbounded fluid domain are shown. Γ_i and Γ_o define the integration lines for calculating the transmitted sound power. (b) Cavity resonant modes. The symmetric mode (lower) termed as mode S and antisymmetric mode (upper) termed as mode AS, where p_r denotes the real part of the total pressure normalized to its maximum value.

Kronowetter *et al.*, 2020). Furthermore, the symmetric and antisymmetric cavity resonant modes, exhibiting in- and anti-phase oscillation of the two resonators, are depicted in Fig. 1(b). The cavity resonant modes are identified as the two modes with the highest quality factors ($Q = f/2|\gamma|$). The corresponding cavity resonant frequencies will be discussed in the following section. In addition, we use the integration lines for the transmission response evaluation at Γ_i and Γ_o. Their positions are chosen such that they match the experimental microphone locations.

III. RESULTS

A. Inter-resonator distance

The first influence parameter to be examined is the distance l between two identical resonators, varied from $l = 2$ mm to $l = 300$ mm. Figures 2(a) and 2(b) show the real and imaginary parts of the complex eigenfrequencies f_c associated with cavity resonance as a function of l. The real parts of the eigenfrequencies associated with cavity resonance oscillate around a reference frequency of $f = 1960$ Hz. The oscillation period matches the resonant wavelength $\lambda = 175$ mm, similar to the Fabry–Pérot interference observed by Hein *et al.* (2012) for duct-cavity systems. Thus, the two modes cross at periodic distances of $\Delta l = \lambda/2$. The crossing points of real parts [Fig. 2(a)] and imaginary parts [Fig. 2(b)] are shifted by about a quarter wavelength. Consequently, the imaginary parts split where the real parts cross and *vice versa*. The mode with the smaller imaginary part γ has increased lifetime and dominates the decay process in the time domain, whereas it leads to a higher sound attenuation in the frequency domain.
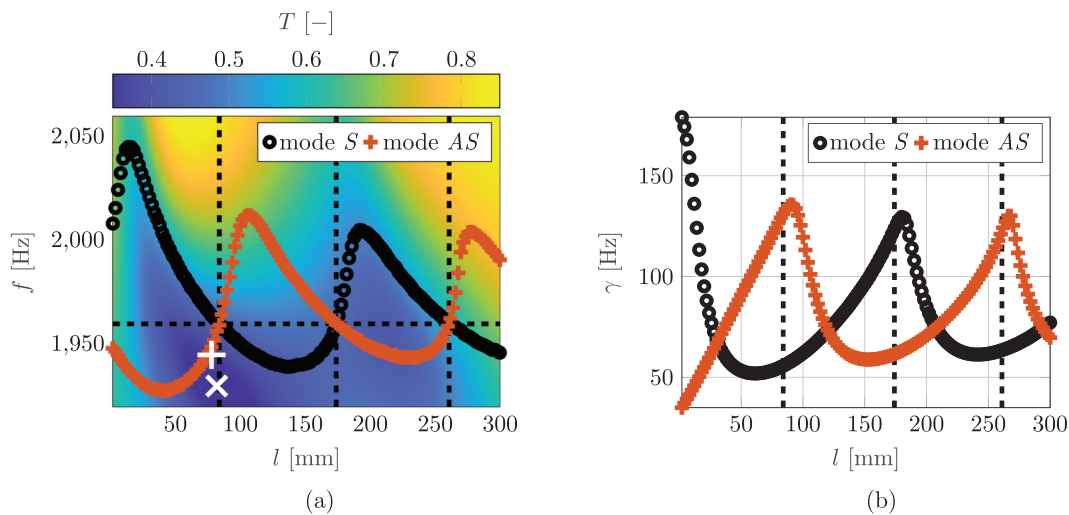
FIG. 2. (Color online) (a) Real and (b) imaginary parts of the complex eigenfrequencies f_c associated with cavity resonance as a function of the inter-resonator distance l (mm). The dashed black lines indicate the distances of the modal crossings and modal (anti-) crossings. The color bar represents the values of the transmission efficiency T (-). The white plus sign (lossless) and white cross (including thermo-viscous losses) mark the points where the transmission efficiencies reach their minima.

The phase difference between resonators is $\Delta\Theta = \pm\pi$ for the antisymmetric mode and zero for the symmetric mode, independent of the inter-resonator distance.

Based on the modal analysis, the highest attenuation of an incident sound wave is expected at the crossing points of in- and anti-phase modes. On the one hand, the dominant mode—the mode with the lowest imaginary part—has the highest quality factor just below the degeneracy, which is the reason for the minimum in the transmission spectrum. On the other hand, detuning decreases the quality factor of the dominant mode. We can say that the modal degeneracy is a prerequisite for particularly high transmission minima and thus for increased local energy trapping. Figure 2(a) shows the transmission efficiency $T = P_o/P_i$ —where P_o is the total transmitted sound power evaluated at Γ_o and P_i is the power of the incident wave evaluated at Γ_i—as a function of separation l and frequency f of the incident plane wave, including thermo-viscous losses.

The drops in the transmitted sound power are located around every second modal crossing point and extend along the frequency of the descending mode. This means that the attenuation reaches its maximum where the symmetric mode dominates. In the regions with dominating antisymmetric mode, transmitted sound power does not decrease. Sawicki et al. (2018) show in case of organ pipes that for zero detuning, the in-phase mode ($\Delta\theta = 0$) corresponds to enhancement and the anti-phase mode ($\Delta\theta = \pi$) corresponds to a cancellation of sound. We can see that the white plus sign in Fig. 2(a) is shifted from $l = 78$ mm and $f = 1945$ Hz to the white cross at $l = 82$ mm and $f = 1930$ Hz just by considering losses. Hence, losses lead to a frequency and distance shift of the minimum transmitted sound power and are considered in the following time harmonic studies.

The reason for the drop in the transmitted sound power at modal crossing points with the dominant symmetric mode is the different coupling between the two modes and the incident plane wave. Modal degeneracy means that any superposition of the two interacting modes will have the same resonant dynamic behavior. In the present configuration, the symmetric mode dominates because both resonators are excited in phase by a plane wave that is normally incident on them. When the angle of incidence is changed by 90° with respect to the initial configuration in Fig. 1(a), there is a slight decrease in the transmitted sound power for the dominant antisymmetric mode. The coupled modes of the system are always linked. In particular, the minimum decay of the symmetric mode occurs near the degeneracy, and also near the maximum decay of the antisymmetric mode.

B. Relative orientation

The second influence factor to be examined is the C-shapes' relative orientation. It is known to be relevant in electromagnetic metamaterials, as shown by the findings of Powell et al. (2011). In addition, earlier research results by Powell et al. (2010) and Hesmer et al. (2007) suggest that the relative orientation plays a major role for the coupling of SRRs. It may therefore also be of importance for the acoustic counterpart. Starting with facing apertures for zero twist angle $\alpha = 0°$, the two C-shapes are rotated in opposite directions and reach the configuration in Fig. 1(a) for $\alpha = 90°$. A maximum twist angle of $\alpha = 180°$ implies that the two apertures are pointing away from each other.

Figure 3(a) shows the absolute difference between the cavity resonant frequencies $\Delta f = |f_1 - f_2|$ in the parameter plane of inter-resonator distance l and twist angle α.

The dark blue regions indicate the course of the modal crossings (depicted by the red line) with $\Delta f = 0$. Regarding the coupling mechanism, the distance between the apertures is a relevant parameter. However, there has to be an
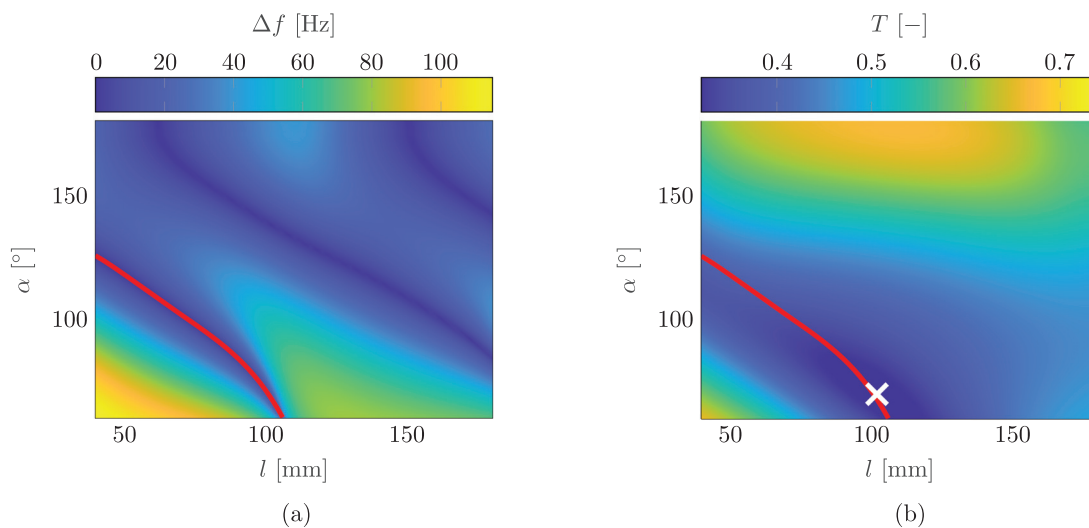

FIG. 3. (Color online) (a) Difference between the real parts of the cavity resonant frequencies $\Delta f = |f_1 - f_2|$ of mode S and AS in the plane of inter-resonator distance l (mm) and angle α (°). The modal crossings are represented by the dark blue lines with zero frequency difference $\Delta f = 0$. The black line indicates a constant inter-aperture distance l_a starting at the second crossing point for $\alpha = 0°$. (b) Transmission efficiency T (-) for a plane wave with $f = 1930$ Hz in the plane of inter-resonator distance l (mm) and angle α (°). The minimum transmission efficiency is highlighted by the white cross. (a) and (b) For comparison, the first modal crossing is indicated by red lines in both figures.

J. Acoust. Soc. Am. **154** (2), August 2023

Kronowetter et al. 845

additional effect besides the changing distance between the apertures. The C-shapes can be regarded as Helmholtz resonators embedded within a cylinder (Melnikov *et al.*, 2019). Thus, the background scattering of the cylinders also plays a major role. The impact of the scattering on the interaction between the resonators is negligible for facing apertures ($\alpha = 0°$) and grows with the twist angle, as the apertures move away from each other. A detailed analysis of the background scattering exceeds the scope of this work.

As observed in Fig. 2(a), the modal crossings provide the locations of possible transmission minima, that is attenuation maxima. The transmission efficiency T in the plane of inter-resonator distance l and twist angle α is shown in Fig. 3(b). The incident wave has a frequency of $f = 1930$ Hz, matching the frequency of the lowest transmission efficiency marked by the white cross in Fig. 2(a). As a result, transmission dips and modal crossings occur at the same distances and twist angles. For comparison, the first modal crossings are indicated by red lines in both plots in Fig. 3. Like in Fig. 2(a), the transmission dips only occur where the symmetric mode dominates, because of the relative orientation of resonators and incident wave.

The dark blue regions with $\Delta f = 0$ in Fig. 3(a) cover all considered inter-resonator distances. This means that the modal crossings can be shifted to arbitrary resonator separations by varying the relative orientation of the two C-shapes. Independent of the orientation, the period is maintained. The transmission results show that the attenuation maxima follow the modal crossings. Thus, the combination of the two parameters, distance and orientation, offers the possibility of reaching attenuation maxima for a prescribed distance or lattice constant by adjusting the orientation and *vice versa*. Surprisingly, the attenuation maxima for this configuration is not found at $\alpha = 90°$ but at $\alpha = 70°$ and $l = 102$ mm. Similar results are observed by additionally varying the frequency of the incoming wave.

C. Frequency detuning and radiation losses

Another influencing factor is the frequency detuning $\Delta = (f_B - f_A)/f_A$. Therefore, we detune the resonance frequency of one of the C-shaped resonators by adjusting the geometrical parameters (r, w, t) before coupling them together. Often associated with synchronization theory (Pikovsky *et al.*, 2001), frequency detuning is a measure for the difference between the uncoupled natural frequencies of two oscillators A and B. In synchronization theory, nonlinear effects can overcome detuning, but for our linear case, we can still observe degeneracy in certain cases. Detuning can arise due to fabrication imperfections, for example. In the following, it is set to $\Delta = 3\%$. Resonator A remains unchanged with a constant resonant frequency of $f_A = 1960$ Hz and resonator B is scaled such that $f_B = 2020$ Hz.

Like the case of zero detuning, the complex eigenfrequencies and the modal phase differences provide information about the coupling mechanism. The real and imaginary parts of the complex eigenfrequencies f_c associated with cavity resonance for variable resonator separation l are plotted in Figs. 4(a) and 4(b).

Except for the first crossing point of Fig. 2(a), the two modes no longer cross in the real part. The modal resonant frequencies still converge every half average wavelength $\Delta l = \bar{\lambda}/2$ with $\bar{\lambda} = (\lambda_A + \lambda_B)/2$, like in the case of zero detuning in Fig. 2(a). However, they do not become identical, but pass through an avoided crossing and then diverge again. The resulting anti-crossing gap grows with increasing distance, that is, with decreasing coupling strength. In contrast, the imaginary parts of the eigenfrequencies exhibit an additional modal crossing at the distance of the anti-crossing in the real part. Thus, they cross-every $\Delta l = \bar{\lambda}/4$.

The influence of a frequency mismatch on the occurrence of degenerate modes can be explained by varying the detuning at the points of degeneracy for zero detuning. More precisely, the detuning is varied from $\Delta = \pm 15\%$ at the distances of the first two points of degeneracy for zero detuning, previously shown in Fig. 2(a), and furthermore, at the distance of the second crossing of the imaginary parts in Fig. 2(b). Figure 5 shows the real and imaginary parts of the complex eigenfrequencies f_c associated with cavity resonance as a function of the detuning Δ at $l = 84$, 120, 174 mm, respectively.

FIG. 4. (Color online) (a) Real and (b) imaginary parts of the complex eigenfrequencies f_c associated with cavity resonance as a function of the inter-resonator distance l (mm) with frequency detuning $\Delta = 3\%$. The dashed black lines indicate the distances of the modal crossings and modal (anti-) crossings extracted from Fig. 2(a).

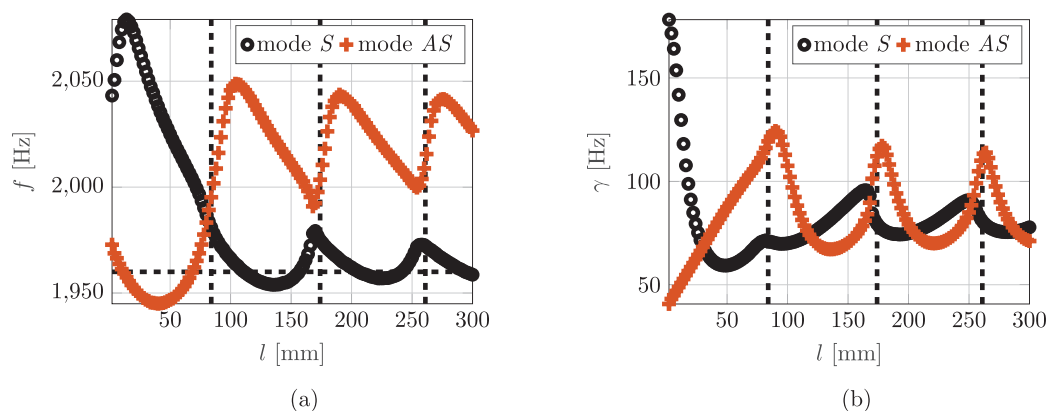846   J. Acoust. Soc. Am. **154** (2), August 2023
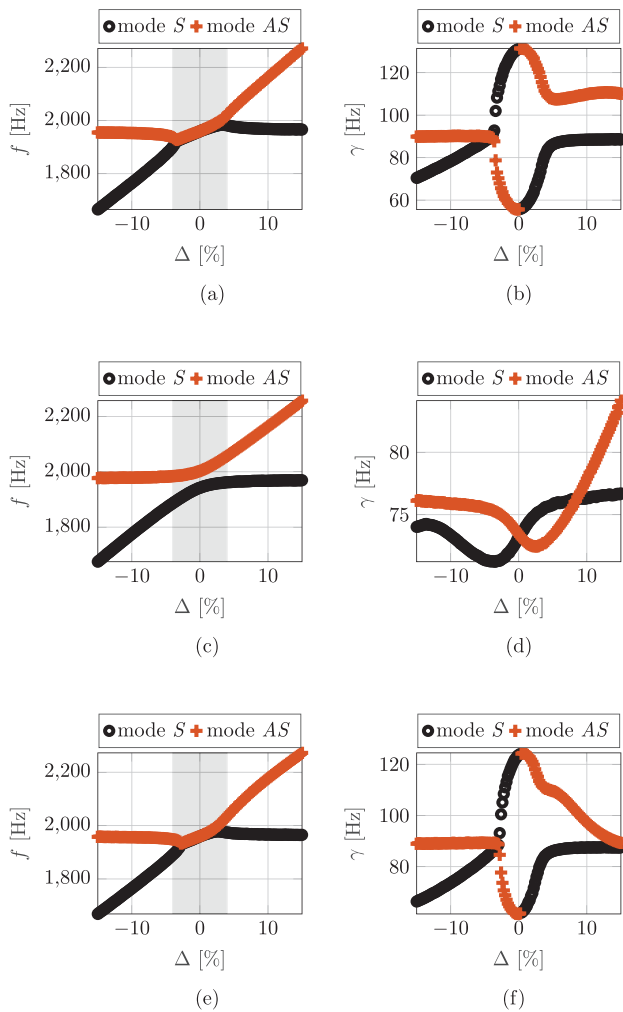
Kronowetter *et al.*

FIG. 5. (Color online) Real and imaginary parts of the complex eigenfrequencies f_c associated with cavity resonance as a function of the frequency detuning Δ [%] at the first and second point of degeneracy obtained from Fig. 2(a) and at the second crossing point of the imaginary parts in Fig. 2(b). The gray area marks the range of $\pm 3\%$ detuning. (a) real part, $l = 84$ mm, (b) imaginary part, $l = 84$ mm, (c) real part, $l = 120$ mm, (d) imaginary part, $l = 120$ mm, (e) real part, $l = 174$ mm, and (f) imaginary part, $l = 174$ mm.

Looking at the real parts in Figs. 5(a) and 5(e), the region of degeneracy with identical resonant frequencies is clearly visible. In this region, one can expect a destructive interference of the two degenerate modes, which can be observed, e.g., in the transmission spectrum. Figures 5(c) and 5(d) show an avoided crossing in the real parts of the eigenvalues and a point of degeneracy in the imaginary part. We can state that no degenerate modes can be found between crossing points in the real part, even for a detuned system. With decreasing coupling strength, that is, with increasing distance l from Figs. 5(a)–5(e), the region of degeneracy becomes smaller. This explains the previous results for $\Delta = 3\%$ in Fig. 4(a). For very small distances, the coupling is still strong enough to overcome the frequency mismatch and thus cause degeneracy of the modes. As the separation increases, a detuning of $\Delta = 3\%$ no longer lies in the region of degeneracy. The coupling is too weak to merge the two resonant frequencies, resulting in an

avoided crossing. The larger the inter-resonator distance, the larger the anti-crossing gap. As observed before, identical real parts of the eigenfrequencies cause the imaginary parts in Figs. 5(b) and 5(f) to move apart. The curves of the resonant frequencies in Figs. 5(a) and 5(e) agree with the typical curve based on synchronization theory (Pikovsky *et al.*, 2001), even if we do not consider non-linear effects. A similar behavior is observed in the experimental results for a pair of organ pipes by Fischer *et al.* (2016).

Having examined the influence parameters inter-resonator distance l and frequency detuning Δ separately, the final step is their combination. Figure 6 shows the cavity resonant frequency difference $\Delta f = |\Re(\bar{\omega}_1 - \bar{\omega}_2)|$ of mode S and AS as a function of the two variables and we call it the degeneracy pattern. In the resulting parameter plane, the frequency difference is approximately periodic in l-direction and nearly symmetric about $\Delta = 0$. The degeneracy of modes is represented by the dark blue regions (line-shaped regions in Δ-direction) with zero frequency difference $\Delta f = 0$. These line-shaped regions of degeneracy are arranged periodically, with the period corresponding to half the average uncoupled wavelength $\bar{\lambda}/2$. This matches the period expected from the modal (anti-) crossings of the cavity resonant frequencies for varying separations in Figs. 2(a) and 4(a). The lines of degeneracy are slightly inclined towards smaller distances for positive frequency detuning due to smaller periods for smaller average resonant wavelengths. Since this effect accumulates over the distance, it becomes especially visible for larger separations. The first region of degeneracy extends over a wide range of detuning. For the second region, the range becomes smaller and decreases only weakly afterwards. This decrease in width with increasing separation, and thus weaker coupling, is in accordance with the regions of degeneracy in Fig. 5.

If the radiation losses are sufficiently increased for a fixed detuning, the modal crossing can be restored. In case of the C-shaped resonators, the radiation losses can be tuned by aperture width. This becomes obvious when comparing the results for the initial C-shape with $w_A = 4$ mm and an increased aperture width of $w_A = 4.25$ mm for $\Delta = 3\%$ (see Fig. 7).
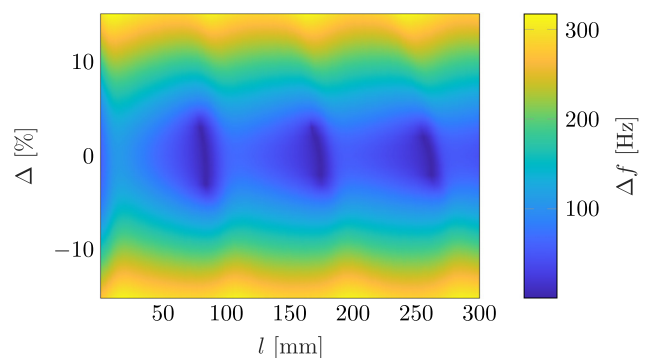
FIG. 6. (Color online) Difference between the real parts of the cavity resonant frequencies $\Delta f = |\Re(\bar{\omega}_1 - \bar{\omega}_2)|$[Hz] of mode S and AS in the plane of inter-resonator distance l (mm) and frequency detuning Δ [%]. The degeneracy pattern shows the degeneracy of modes represented by the dark blue regions $\Delta f = 0$.

J. Acoust. Soc. Am. **154** (2), August 2023

Kronowetter *et al.*   847
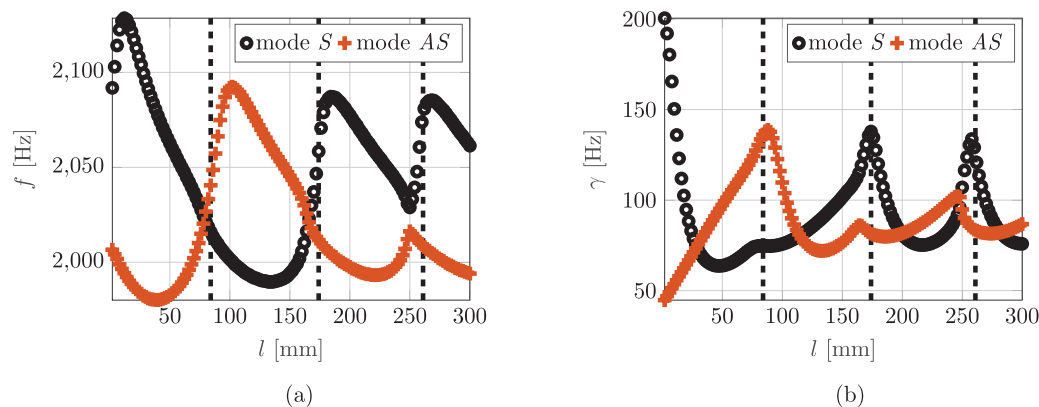
(a)   (b)

FIG. 7. (Color online) (a) Real and (b) imaginary parts of the complex eigenfrequencies f_c associated with cavity resonance as a function of the inter-resonator distance l (mm) with frequency detuning $\Delta = 3\%$, for a geometry with increased radiation losses increased aperture width w_A=4.25 mm, initially w_A=4 mm). The dashed black lines indicate the distances of the modal crossings and modal (anti-) crossings extracted from Fig. 2(a).

Figures 7(a) and 7(b) show the complex eigenfrequencies f as a function of the resonator separation l for the case with increased aperture width, that is, with increased γ of about 10%. Compared to Fig. 4(a), the modal crossings in the real parts are restored, while the imaginary parts approach each other without crossing at these distances, indicated by the dashed black lines. The further the losses are increased, the smoother are the curves in the vicinity of the crossing points.

An illustrative explanation for the counteracting effects can be given looking at the real parts of the cavity resonant frequencies in Figs. 2(a), 4(a) and 7(a). The frequency detuning opens a gap between the uncoupled and coupled resonant frequencies [see Fig. 4(a)]. However, this gap can be bridged by a sufficiently high increase in γ [see

Fig. 7(a)]. As the coupling increases with the radiation losses, it can be tuned by aperture width.

D. Experimental validation

To experimentally valid the acoustic performance of the coupled resonators, the transmission efficiency of two identical C-shaped meta-atoms was measured in a two-dimensional parallel-plate waveguide system as shown in Fig. 8(a).

The meta-atom samples are fabricated using additive manufacturing (3D printing) with polylactide (PLA). The two samples are shown in Fig. 8(b). We create an incident plane wave by using an array of eight loudspeakers. The

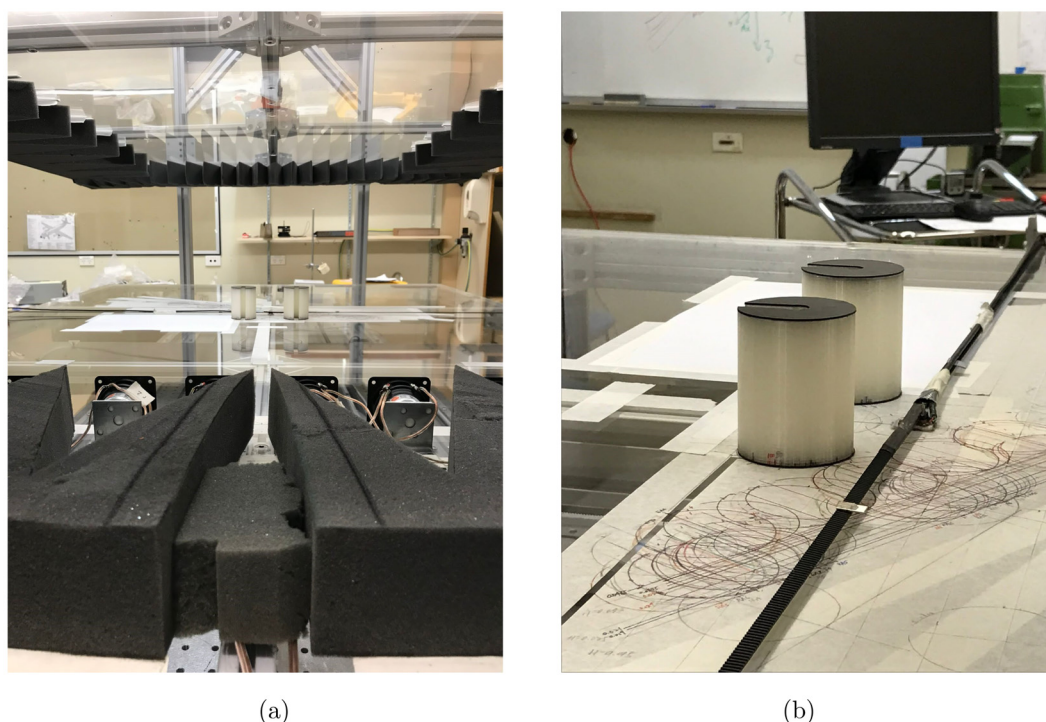

(a)   (b)

FIG. 8. (Color online) Experimental setup. (a) C-shaped meta-atoms placed in waveguide. (b) C-shaped meta-atoms.
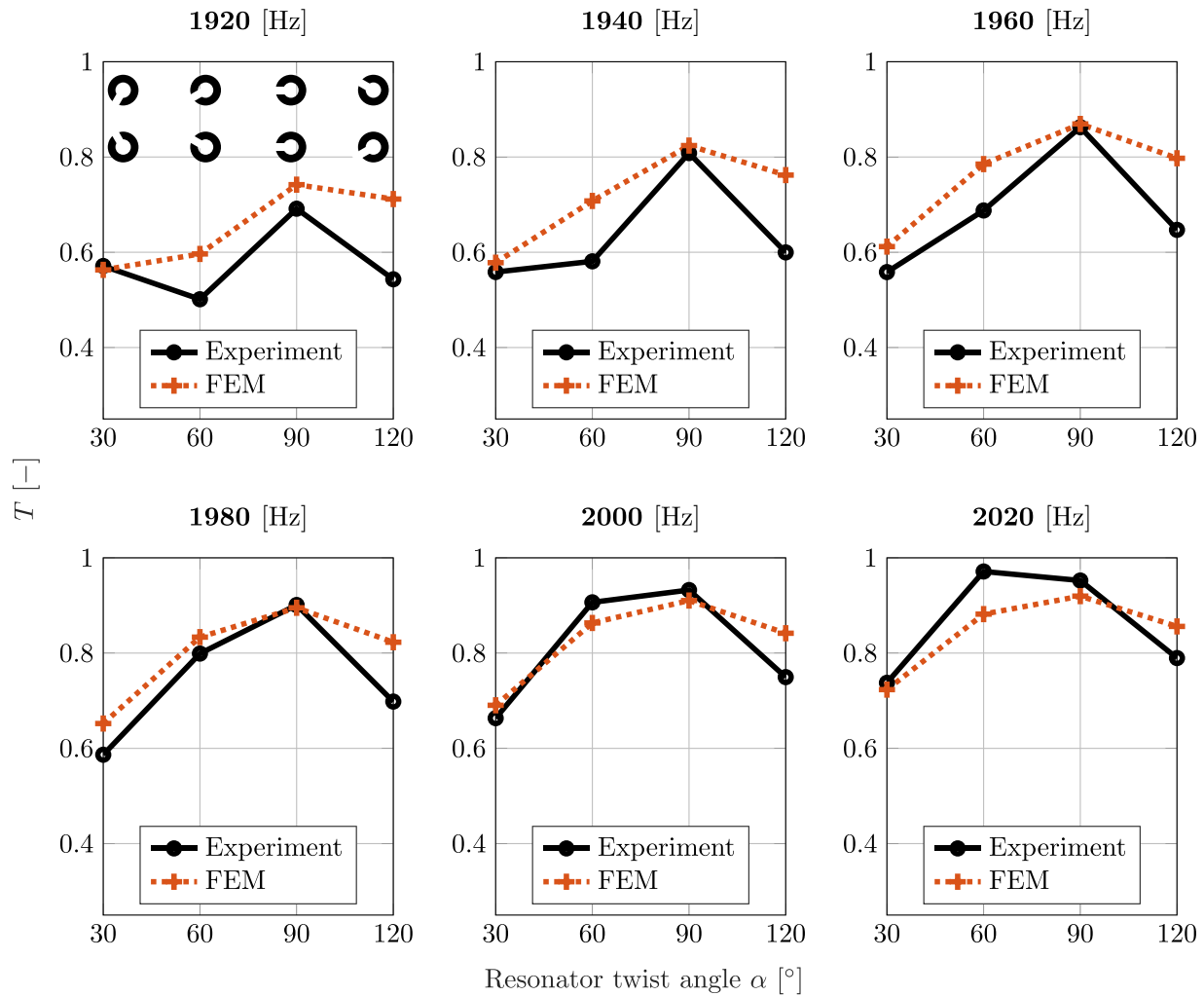
FIG. 9. (Color online) Experimental and numerical transmission efficiencies for six different frequencies evaluated at the twist angels of the resonators $\alpha = 30°$, $60°$, $90°$, and $120°$ and an inter-resonator distance of 60 mm. The configurations of the C-shapes in C-shapes in dependence of the twist angles are presented on the top left.

incident and transmitted fields are measured along a vertical straight line by the microphone mounted on a belt system. The waveguide system is surrounded by absorbing foam to reduce unwanted reflection from the boundaries. We use four different orientations $\alpha = 30°$, $60°$, $90°$, and $120°$ to experimentally demonstrate the sound attenuation of coupled meta-atoms. The sound reduction performance is examined by the transmission efficiency and compared with the numerical results (see Fig. 9).

The measured data match the trend of the simulated data quite well. The minor deviations in the transmission efficiency are due to inaccuracies in the setup, inaccuracies of modelling losses, and also modelling the acoustic source. Our model only covers the acoustic field, and no flow is considered. We also use a background pressure field in the COMSOL model, leading to plane wave excitation, while we use an array of loudspeakers mimicking a plane wave in the experimental setup. Since we are still able to reproduce the characteristic of the transmission efficiency in simulation and experiment, we consider the results as validated by experiment and hence, applicable in a real environment

including all kind of losses. Furthermore, we show that the transmission efficiency strongly depends on the twist angle of the C-shapes at a fixed distance l. The configurations of the C-shapes for the four measured twist angles are presented on the top left of Fig. 9. We control the level of sound attenuation of the coupled C-shapes, for instance, by changing the twist angle from $90°$–$60°$ at an excitation frequency of 1960 Hz. This leads to a decrease in the transmission efficiency from 0.86–0.69. As a result, the measurement results confirm the simulated data and hence, demonstrate the twist angle as parameter to control the level of sound attenuation of the coupled C-shapes.

IV. CONCLUSION

We show that degeneracy of modes for identical C-shaped Helmholtz resonators occurs at periodic distances with either the symmetric or antisymmetric mode dominating. By introducing detuning, we demonstrate that modal degeneracy depends on the level of detuning and on the coupling strength. Modal degeneracy can still occur for weak enough

detuning at certain specific distances between the resonators and, moreover, leads to the highest sound attenuation.

This region of degeneracy has similarities to Arnold tongues in non-linear synchronization theory. The degeneracy of modes holds within a certain range of frequency detuning—the region of degeneracy. Its scope narrows with increasing inter-resonator distance, that is, decreasing coupling strength. At the edge of the region of degeneracy, the phase differences converge to $\Delta\Theta = \pm\pi/2$. For varying distances, detuning values outside the degeneracy region lead to periodic avoided modal crossings of the real parts of the eigenfrequencies. The imaginary parts of the eigenfrequencies cross at the location of the avoided crossings of the real parts. At the distances of these (avoided) crossings, also the phase differences cross. This indicates an interchange in the nature of the two modes.

For C-shaped resonators, the radiation losses can be tuned by aperture width and counteract the effect of detuning. The combined effect of distance and detuning becomes visible in the degeneracy pattern. It consists of line-shaped regions of degeneracy, which are periodic in distance–direction and symmetric about zero detuning.

Furthermore, coupling induces the possibility of tuning via the resonators' relative arrangement, that is, distance and orientation. Starting with facing apertures, the two resonators were twisted in opposite directions. Thereby, the degeneracy of modes can be shifted to arbitrary distances, while the period is maintained. The location of the crossing points depends on the inter-aperture distance and is additionally influenced by background scattering effects. Moreover, the relative orientation affects the width of the regions of degeneracy. This means that the coupling strength depends on relative orientation and distance. Accordingly, these two influence parameters offer additional degrees of freedom for tuning the metamaterial response with unchanged components.

We also use coupled mode theory as an analytical approach to determine the coupling coefficient, but do not present it throughout the manuscript. The reason for this is that any asymmetry depends on the off diagonal terms, which makes the eigenvalue problem quite complicated. Determining the coupling coefficients using analytical models could be the subject of future research.

Experiments in a two-dimensional parallel-plate waveguide were conducted, showing good agreement and hence, validating the numerical results. In addition to their validation, the presented findings provide a base for further research, in particular, concerning the application to acoustic metamaterials.

The impact of the resonators' relative arrangement on the interaction and hence, the metamaterial response, provides additional degrees of freedom for the design of metamaterials. Since we can significantly manipulate the transmission efficiency of the coupled meta-atoms by changing the twist angle, our results offer new possibilities for more efficient and versatile metamaterials for noise control. In addition, our findings help drive progress in the design of advanced and high-performance metamaterials for a wide range of applications besides sound barriers.

Al Jahdali, R., and Wu, Y. (**2018**). "Coupled resonators for sound trapping and absorption," Sci. Rep. **8**, 13855.

Baydoun, S. K., and Marburg, S. (**2020**). "Investigation of radiation damping in sandwich structures using finite and boundary element methods and a nonlinear eigensolver," J. Acoust. Soc. Am. **147**(3), 2020–2034.

Belacel, C., Todorov, Y., Barbieri, S., Gacemi, D., Favero, I., and Sirtori, C. (**2017**). "Optomechanical terahertz detection with single meta-atom resonator," Nat. Commun. **8**, 1578.

Cavalieri, T., Cebrecos, A., Groby, J.-P., Chaufour, C., and Romero-García, V. (**2019**). "Three-dimensional multiresonant lossy sonic crystal for broadband acoustic attenuation: Application to train noise reduction," Appl. Acoust. **146**, 1–8.

Chalmers, L., Elford, D. P., Kusmartsev, F. V., and Swallowe, G. M. (**2009**). "Acoustic band gap formation in two-dimensional locally resonant sonic crystals comprised of Helmholtz resonators," Int. J. Mod. Phys. B. **23**(20-21), 4234–4243.

COMSOL Inc. (**2021**). "COMSOL Multiphysics v5.6."

Cummer, S. A., Christensen, J., and Alù, A. (**2016**). "Controlling sound with acoustic metamaterials," Nat. Rev. Mater. **1**(3), 16001.

Deymier, P. A. (**2013**). Acoustic Metamaterials and Phononic Crystals (Springer, Heidelberg, Germany), available at https://link.springer.com/book/10.1007/978-3-642-31232-8.

Dong, Y., Yu, G., Wang, X., Niu, X., Wu, K., and Wang, N. (**2017**). "Broadband and wide-angle blazed acoustic gratings using multiple coupled Helmholtz resonators," Appl. Phys. Express **10**(9), 097201.

Dukhin, A., and Goetz, P. (**2002**). Ultrasound for Characterizing Colloids: Particle Sizing Zeta Potential Rheology, 1st ed. (Elsevier, Boston).

Elford, D. P., Chalmers, L., Kusmartsev, F. V., and Swallowe, G. M. (**2011**). "Matryoshka locally resonant sonic crystal," J. Acoust. Soc. Am. **130**(5), 2746–2755.

Fang, N., Xi, D., Xu, J., Ambati, M., Srituravanich, W., Sun, C., and Zhang, X. (**2006**). "Ultrasonic metamaterials with negative modulus," Nat. Mater. **5**(6), 452–456.

Fischer, J. L., Bader, R., and Abel, M. (**2016**). "Aeroacoustical coupling and synchronization of organ pipes," J. Acoust. Soc. Am. **140**(4), 2344–2351.

Fu, Y. H., Liu, A. Q., Zhu, W. M., Zhang, X. M., Tsai, D. P., Zhang, J. B., Mei, T., Tao, J. F., Guo, H. C., Zhang, X. H., Teng, J. H., Zheludev, N. I., Lo, G. Q., and Kwong, D. L. (**2011**). "A micromachined reconfigurable metamaterial via reconfiguration of asymmetric split-ring resonators," Adv. Funct. Mater. **21**(18), 3589–3594.

Hein, S., Koch, W., and Nannen, L. (**2012**). "Trapped modes and Fano resonances in two-dimensional acoustical duct-cavity systems," J. Fluid Mech. **692**, 257–287.

Herrero-Durá, I., Cebrecos, A., Picó, R., Romero-García, V., García-Raffi, L. M., and Sánchez-Morcillo, V. J. (**2020**). "Sound absorption and diffusion by 2D arrays of Helmholtz resonators," Appl. Sci. **10**(5), 1690.

Hesmer, F., Tatartschuk, E., Zhuromskyy, O., Radkovskaya, A., Shamonin, M., Hao, T., Stevens, C., Faulkner, G., Edwards, D., and Shamonina, E. (**2007**). "Coupling mechanisms for split ring resonators: Theory and experiment," Phys. Status Solidi B **244**, 1170–1175.

Jiang, X., Li, Y., and Zhang, L. (**2017**). "Thermoviscous effects on sound transmission through a metasurface of hybrid resonances," J. Acoust. Soc. Am. **141**(4), EL363–EL368.

Johansson, T. A., and Kleiner, M. (**2001**). "Theory and experiments on the coupling of two Helmholtz resonators," J. Acoust. Soc. Am. **110**(3), 1315–1328.

Jordaan, J., Punzet, S., Melnikov, A., Sanches, A., Oberst, S., Marburg, S., and Powell, D. A. (**2018**). "Measuring monopole and dipole polarizability of acoustic meta-atoms," Appl. Phys. Lett. **113**(22), 224102.

Keiser, G. R., Fan, K., Zhang, X., and Averitt, R. D. (**2013**). "Towards dynamic, tunable, nonlinear metamaterials via near field interactions: A review," J. Infrared. Millim. Terahertz Waves **34**(11), 709–723.

Krasikova, M., Krasikov, S., Melnikov, A., Baloshin, Y., Marburg, S., Powell, D. A., and Bogdanov, A. (**2023**). "Metahouse: Noise-insulating chamber based on periodic structures," Adv. Mater. Technol. **8**, 2200711.

Kronowetter, F., Baydoun, S. K., Eser, M., Moheit, L., and Marburg, S. (**2020**). "A benchmark study on eigenfrequencies of fluid-loaded structures," J. Theor. Comput Acoust. **28**(02), 2050013.

Lee, T., and Iizuka, H. (**2019**). "Bragg scattering based acoustic topological transition controlled by local resonance," Phys. Rev. B **99**, 064305.

Liu, H., Liu, Y. M., Li, T., Wang, S. M., Zhu, S. N., and Zhang, X. (**2009a**). "Coupled magnetic plasmons in metamaterials," Phys. Status Solidi B **246**(7), 1397–1406.

850   J. Acoust. Soc. Am. **154** (2), August 2023

Kronowetter et al.

Liu, N., Liu, H., Zhu, S., and Giessen, H. (**2009b**). "Stereometamaterials," Nat. Photon. **3**(3), 157–162.

Ma, G., and Sheng, P. (**2016**). "Acoustic metamaterials: From local resonances to broad horizons," Sci. Adv. **2**(2), e1501595.

Melnikov, A., Chiang, Y. K., Quan, L., Oberst, S., Alù, A., Marburg, S., and Powell, D. (**2019**). "Acoustic meta-atom with experimentally verified maximum Willis coupling," Nat. Commun. **10**(1), 3148.

Milton, G. W., and Willis, J. R. (**2007**). "On modifications of Newton's second law and linear continuum elastodynamics," Proc. R. Soc. A. **463**(2079), 855–880.

Movchan, A. B., and Guenneau, S. (**2004**). "Split-ring resonators and localized modes," Phys. Rev. B **70**(12), 125116.

Pendry, J. B. (**2000**). "Negative refraction makes a perfect lens," Phys. Rev. Lett. **85**(18), 3966–3969.

Pendry, J. B., Schurig, D., and Smith, D. R. (**2006**). "Controlling electromagnetic fields," Science **312**(5781), 1780–1782.

Pikovsky, A., Rosenblum, M., and Kurths, J. (**2001**). *Synchronization: A Universal Concept in Nonlinear Sciences*, Cambridge Nonlinear Science Series (Cambridge University Press, Cambridge, UK).

Powell, D. A., Hannam, K., Shadrivov, I. V., and Kivshar, Y. S. (**2011**). "Near-field interaction of twisted split-ring resonators," Phys. Rev. B **83**(23), 235420.

Powell, D. A., Lapine, M., Gorkunov, M. V., Shadrivov, I. V., and Kivshar, Y. S. (**2010**). "Metamaterial tuning by manipulation of near-field interaction," Phys. Rev. B **82**(15), 155128.

Sawicki, J., Abel, M., and Schöll, E. (**2018**). "Synchronization of organ pipes," Eur. Phys. J. B **91**(2), 1–9.

Schurig, D., Mock, J. J., Justice, B. J., Cummer, S. A., Pendry, J. B., Starr, A. F., and Smith, D. R. (**2006**). "Metamaterial electromagnetic cloak at microwave frequencies," Science **314**(5801), 977–980.

Strutt, J. W. (**2011**). *The Theory of Sound*, Cambridge Library Collection - Physical Sciences (Cambridge University Press, Cambridge, UK).

Valentine, J., Li, J., Zentgraf, T., Bartal, G., and Zhang, X. (**2009**). "An optical cloak made of dielectrics," Nat. Mater. **8**(7), 568–571.

Wang, Y.-F., and Laude, V. (**2017**). "Longitudinal near-field coupling between acoustic resonators grafted onto a waveguide," Crystals **7**, 323.

Wu, L., Xi, X., Li, B., and Zhou, J. (**2017**). "Dielectric meta-atom with tunable resonant frequency temperature coefficient," Sci. Rep. **7**, 2566.

Yakovlev, A. B., and Hanson, G. (**2000**). "Mode-transformation and mode-continuation regimes on waveguiding structures," IEEE Trans. Microw. Theory Techn. **48**, 67–75.

Yang, X., Yin, J., Yu, G., Peng, L., and Wang, N. (**2015**). "Acoustic superlens using Helmholtz-resonator-based metamaterials," Appl. Phys. Lett. **107**(19), 193505.

Yao, S., Zhou, X., and Hu, G. (**2008**). "Experimental study on negative effective mass in a 1D mass-spring system," New J. Phys. **10**(4), 043020.

Zangeneh-Nejad, F., and Fleury, R. (**2019**). "Active times for acoustic metamaterials," Rev. Phys. **4**, 100031.

Zhou, Y., Fang, X., Li, D., Hao, T., and Li, Y. (**2018**). "Acoustic multiband double negativity from coupled single-negative resonators," Phys. Rev. Appl. **10**, 044006.

17 November 2023 00:00:07